sciendo

*Polish Journal of Chemical Technology, 21, **4**, 98—105, 10.2478/pjct-2019-0045*

Synthesis of an optical catalyst for cracking contaminating dyes in the wastewater of factories using indium oxide in nanometer and usage in agriculture

Ishaq F. E. Ahmed*, Ahmed I. El-Shenawy and Moamen S. Refat

Imam Abdulrahman Bin Faisal University, Department of Chemistry, College of Education, P.O. Box 1982, Dammam, Saudi Arabia
**Corresponding author: e-mail: ismohammed@iau.edu.sa*

Herein, the photocatalytic degradation of the Congo Red (CR) and Crystal Violet (CV) dyes in an aqueous solution were discussed in the presence of an indium(III) oxide (In_2O_3) as optical catalyst efficiency. The caproate bidentate indium(III) precursor complex has been synthesized and well interpreted by elemental analysis, molar conductivity, Fourier transform infrared (FT-IR), UV-Vis, and thermogravimetric (TGA) with its differential thermogravimetric (DTG) studies. The microanalytical and spectroscopic assignments suggested that the associated of mononuclear complex with 1:3 molar ratio (M^{3+}:ligand). Octahedral structure is speculated for this parent complex of the caproate anion, $CH_3(CH_2)_4COO^-$ ligand. The In_2O_3 NPs with nanoscale range within 10–20 nm was synthesized by a simple, low cost and eco-friendly method using indium(III) caproate complex. Indium oxide nanoparticles were formed after calcination of precursor in static air at 600°C for 3 hrs. The structural, grain size, morphological and decolorization efficiency of the synthesized NPs were characterized using the FT-IR, X-ray diffraction (XRD), scanning electron microscopy (SEM), energy dispersive X-ray analysis (EDX) and transmission electron microscopy (TEM) analyses. It was worthy mentioned that the prepared In_2O_3 NPs showed a good photodegradation properties against CR and CV organic dyes during 90 min.

Keywords: Photocatalyst; In_2O_3; precursors; Crystal Violet; Congo Red; NPs.

INTRODUCTION

The organic dyes are a plentiful class of organic compounds that exhibit increased environmental risk. Some of these dyes are harmful and carcinogenic[1]. Interactive dyes are widely used in the textile industry because of its wide variety of color shades, simplicity of application, brilliant colors and minimal energy consumption[2]. More attention has been paid recently to the study of the removal of dyes and pigments from industrial waste and sewage through adsorption using nanomaterials[3, 4]. Organic and inorganic dyes are usually removed by different chemical and physical techniques, such as chemical reaction, electrolysis, reverse osmosis, adsorption, flocculation, ion exchange, membrane filtration, electrochemical destruction, precipitation and many more. Among all these techniques, adsorption technology has been found to be superior to other wastewater treatment techniques in terms of initial cost, simplicity of design, ease of operation and hypersensitivity to toxic substances[5]. Nanomaterials have gained importance in this category due to their expected surface area and improved interactive sites[6].

The coordination of carboxylic acid towards metal ions has been the subject of an intensive research study due to its diverse applications, such as the suitability of metal carboxylic complexes as model systems for mineral sites in organic biochemistry[7, 8]. In literature there are few articles discussed the metal complexation of caproic acid with rare earth metals[9, 10], Cu^{I}/Cu^{II} oxides[11], Th^{4+}, Pb^{2+} and Fe^{3+} [12]. The caproic acid play an important role as an analytical reagent for various metal ions e.g. Zr^{4+}, Cr^{3+}, Mn^{2+}, Ga^{3+} and Al^{3+} in presence of chloroform solvent media and catechol violet indicator[13–15].

Recently, the properties and applications of In_2O_3 oxide nanostructured have been studied on a large scale[16, 17]. Indium(III) oxide display a wide band gap within 3.4–3.7 eV range[18]. It is a suitable candidate for the manufacture of various devices such as field effect transistors, light emitting diodes, blocker in tunnel intersections[19], transparent conductive material in LCDs[20] photovoltaic cells and solar cells[18] gas Sensors[21, 22]. Various methods were used to prepared of In_2O_3 powders in nanostructured form and thin films[23–26]. This study aimed to investigate the crystalline structure, morphology and particle size of the synthesized In_2O_3 using FT-IR, XRD, SEM, EDX and TEM spectroscopic analyses. The photodegradation efficient of In_2O_3 NPs on the contaminated dyes (Congo Red and Crystal violet) in the wastewater were discussed dependently on different physical parameters as contact time, dose of adsorbent (In_2O_3), and pH values. These experimental items were determined by UV-Vis spectrophotometer.

EXPERIMENTAL

Chemicals

The caproic acid ($CH_3(CH_2)_4COOH$) and anhydrous $InCl_3$ were received from Fluka (UK) and Alfa Aesar chemical manufacturing company (USA), respectively. These chemicals used as received.

Analyses

I. Elemental analyses	*By*	Perkin Elmer CHN 2400
II. Indium metal ion percentage	*By*	Gravimetric analyses
III. Molar conductivity	*By*	Jenway 4010 conductivity meter
IV. FTIR spectra	*By*	Bruker FT-IR spectrophotometer
V. Electronic absorption	*By*	UV2-Unicam UV/Vis spectrophotometer
VI. Thermogravimetric	*By*	Shimadzu TGA-50H
VII. X-ray powder diffraction	*By*	XPert Philips X-ray diffractometer

Bereitgestellt von West-Pomeranian University of Technology Szczecin - Biblioteka Główna Zachodniopomorskiego | Heruntergeladen 16.01.20 10:41 UTC

VIII. SEM micrograph	*By*	Jeol Jem-1200 EX II Electron microscope
IX. TEM micrograph	*By*	JEOL 100s transmission electron microscope

Synthesis of indium(III) caproate complex

Indium(III) chloride (3 mmol, 0.664 g) was dissolved in 20 mL of bi-distilled water then mixed to 30 mL of an aqueous solution of caproic acid (9 mmol, 1.1 mL) with contentiously stirring. The mixture was neutralized at pH = 7.5 using ammonia solution (10%). The mixture was refluxed at 60°C for 2 hrs, then left to evaporate at room temperature overnight. The yellowish white precipitate was filtered, wash with hot water and little amount methanol solvent and dried at 60°C. [In-$(CH_3(CH_2)_4COO)_3$] complex, Anal.: (Calc.) Found, %: C, (46.97) 46.55; H, (7.23) 7.19; In, (24.95) 24.71; yield 82%; $\Lambda_M = 2.1\ \Omega^{-1}.cm^2.mol^{-1}$.

Synthesis of the In_2O_3 NPs

Calcination of the $[In(CH_3(CH_2)_4COO)_3]$ complex as a precursor material at temperature up to 600°C gives rise to nanocrystalline particles of In_2O_3 with nanoscale size.

Photocatalytic degradation experiment

A 250 mL conical flask including a 100 mL solution of the Congo Red or Crystal violet (Fig. 1) in water (50 mg · L^{-1}) and (50 mg) of synthesized In_2O_3 NPs. While the solution was stirred for approximately 1½ hrs and then exposed to a UV lamp. The absorbances were measured each 15 min. in a spectrophotometer at the maximum wavelength for the Congo Red (498 nm) or Crystal violet (590 nm). The decolorization rate of the dye was determined as expressed in Eq. (1):

$$\text{Dye decolorization, } \% = (A_0 - A_t)/\ A_0 \cdot 100 \qquad (1)$$

Where A_t is the absorbance at requested time and A_0 is the initial absorbance of each solution.

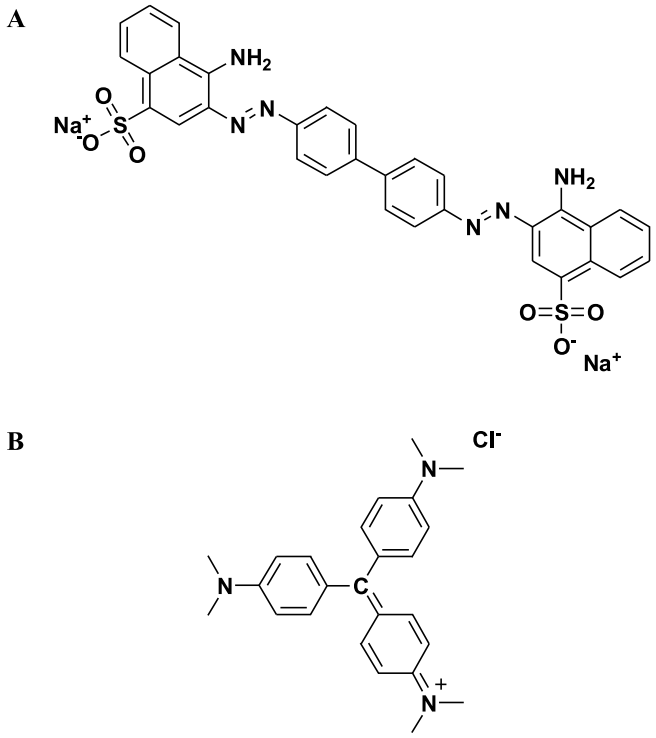

Figure 1. Chemical structures of A: Congo Red (CR) and B: Crystal violet (CV) dyes

RESULTS AND DISCUSSION

Characterization of $[In(CH_3(CH_2)_4COO)_3]$ complex precursor

The main objective from the synthesized of indium(III) caproate complex is to be acquired of good precursors to prepared In_2O_3 oxide in nanostructure form. The new $[In(CH_3(CH_2)_4COO)_3]$ complex precursor was synthesized and well characterized using microanalytical, (FT-IR, UV--Vis) spectroscopy, thermal analyses. Elemental analyses results as seen from these data (experimental section), 1:3 (In : Ligand) binary complex was associated with good agreement matching between experimental and theoretical values. The results indicate that $CH_3(CH_2)_4COOH$ ligand behave as uninegative bidentate molecule. This lose the carboxylate hydrogen atom on complexity with the indium(III) ion. The preparation of this binary complex (Fig. 2) can be proceed as follows:

$$InCl_3 + 3CH_3(CH_2)_4COOH \rightarrow [In(CH_3(CH_2)_4COO)_3] + 3HCl$$

The structure of the indium(III) caproate complex suggested form the elemental analyses agree well with their proposed formula. The solubility of this complex display that its insoluble in most organic solvents (e.g. $CHCl_3$, C_6H_6, CH_3OH, but soluble in DMF and DMSO solvents. The $[In(CH_3(CH_2)_4COO)_3]$ complex is dissolved in DMF and the molar conductivity of 10^{-3}M solution at 30 °C is measured. It is deduced from the experimental result ($2.1\ \Omega^{-1}.cm^2.mol^{-1}$) that the indium(III) precursor complex is 1:3 nonelectrolyte[27].

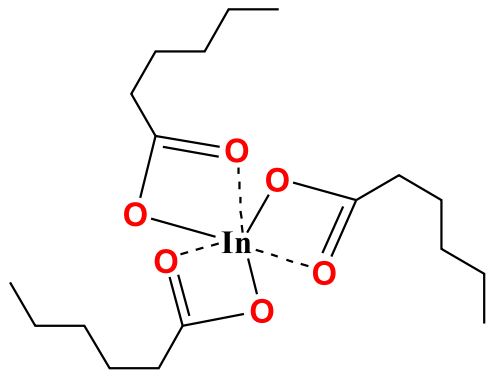

Figure 2. Chemical structure of indium(III) caproate complex

The FT-IR spectrum of the synthesized indium(III) caproate complex is shown in Figure 3. The FT-IR spectrum of free caproic acid, $CH_3(CH_2)_4COOH$, display strong frequency band at 1700 cm^{-1} that is assigned to vibration motion of carbonyl νC = O of (COOH) group. This band is disappeared in case of FT-IR spectrum of the $[In(CH_3(CH_2)_4COO)_3]$ complex and it has been replaced by two new vibration bands at 1549 and 1402 cm^{-1} which are attributed to the asymmetric and symmetric vibration motions of the COO group, respectively[28–30]. Literature survey revealed that the carboxylate group can be chelated with any metal ions by three coordination modes as monodentate (Δν > ionic form), bidentate (Δν < ionic form) or bridged bidentate (Δν ≈ ionic form) that $\Delta\nu = \nu_{as}COO\text{-}\nu_{s}COO)$[1]. In case of infrared spectrum of indium(III) caproate complex, the Δν difference frequencies is 147 cm^{-1}. This value concluded

Bereitgestellt von West-Pomeranian University of Technology Szczecin - Biblioteka Główna Zachodniopomorskiego | Heruntergeladen 16.01.20 10:41 UTC

that the carboxylate group coordinated to indium(III) ion through two oxygen atoms as bidentate binding mode[1, 2] (Fig. 2). There are two new absorption bands at 580 and 454 cm^{-1} attributed to the ν(In-O) frequencies[30].

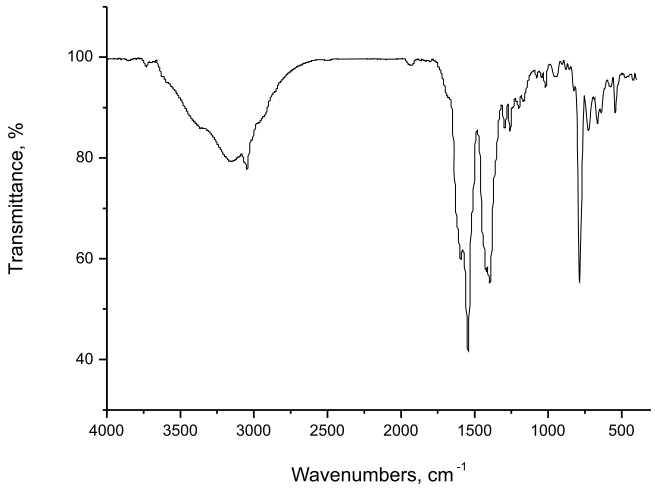

Figure 3. FT-IR spectrum of $[In(CH_3(CH_2)_4COO)_3]$ complex

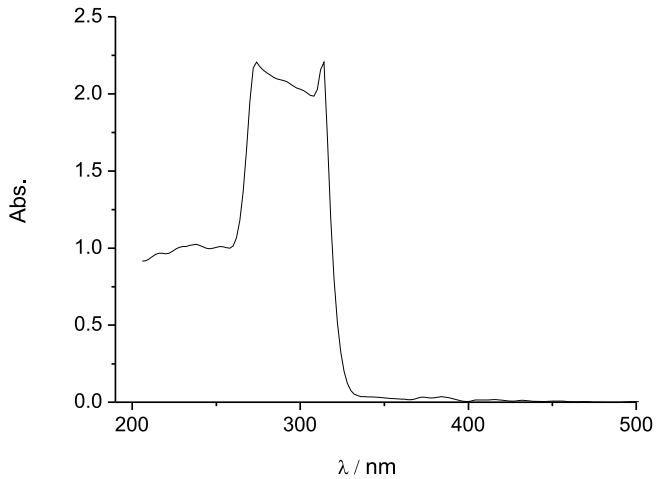

Figure 4. UV-Vis spectrum of $[In(CH_3(CH_2)_4COO)_3]$ complex

The absorption spectrum of the free $CH_3(CH_2)_4CO$-OH acid ligand displayed two bands at 225 and 265 nm that were assigned to π → π* and n → π* transitions of alkyl group (-CH_3 and -CH_2) and carboxylic groups, respectively[31]. Normal absorption spectrum of indium(III) caproate complex (Fig. 4) show maximum absorption bands at l_{max} = 237, 252, 274, 314, and 383 nm. The UV bands at 314 and 383 nm are attributed to metal charge--transfer and d–d transition[32–34]. The relative increases in absorbance due to complex association at 274 and 314 nm. This resulted data was supported the coordination of indium(III) ions via COOH group.

Thermal decomposition of indium(III) caproate complex was investigated based on controlled heating rate at 10°C min^{-1} under nitrogen atmosphere and weight loss was measured from room temperature until 800°C. The TG-DTG curves (Fig. 5), displayed that the thermal degradation of $[In(CH_3(CH_2)_4COO)_3]$ complex passed in a broad peak at DTG_{max} = 499°C. The total mass loss (Calc. 71.59 %, found 71.40 %) was attributed to the elimination of the three caproate organic parts of the indium(III) caproate complex. It is worthy mentioned that, indium(III) caproate complex decompose to ½In_2O_3 oxide but the In(III) caproate complex has an intermediate step due to the association of indium(III) carbonate, $In_2(CO_3)_3$, at about 350°C. This hypothesis is supported by the FT-IR spectrum (Fig. 6) resulted from calcinations of the indium(III) caproate complex at 350°C, as refereed in Figure 6. So that, the proposed thermal degradation equation 2 is:

$$[In(CH_3(CH_2)_4COO)_3] \rightarrow In_2(CO_3)_3 \rightarrow In_2O_3 \text{ Eq.} \quad (2)$$

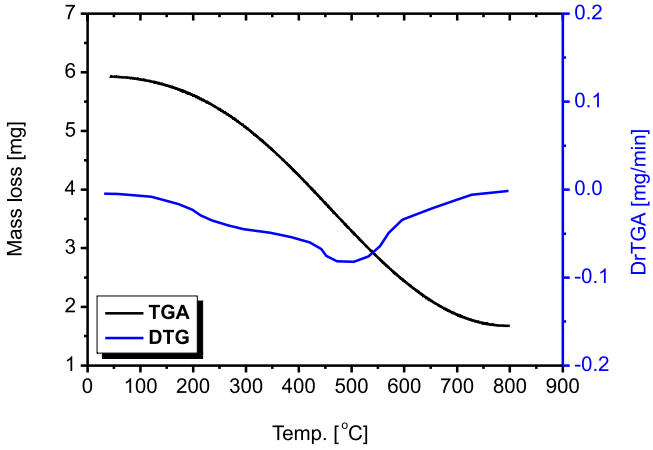

Figure 5. TGA diagram of $[In(CH_3(CH_2)_4COO)_3]$ complex

The kinetic thermodynamic parameters (DG/$kJmol^{-1}$, DH/$kJmol^{-1}$, DS/$Jmol^{-1}K^{-1}$, Z/s^{-1}, E/$kJmol^{-1}$) have been elucidated for the differential thermogravimetric step DTG_{max} 499°C using Coats-Redfern[35] and Horowitz--Metzger[36] methods (Fig. 7). Both values of activation energy E* and entropy DS* of the reaction have been calculated using both methods and found to be in close agreement. The order of reaction in each case is one. The enthalpy of reaction has been calculated, using the TG[37] and DTG curves, respectively[38, 39]. The kinetic parameters for the thermal decomposition of the indium(III) caproate complex are given in Table 1. The activation energy of decomposition was found to be in the range 70–52.8 $kJmol^{-1}$. This high value of the activation energy reflect the thermal stability of the indium(III) caproate complex. The reaction for which ΔG is positive and ΔS is negative considered as unfavorable or as a non spontaneous reaction. The entropy of activation was found to have negative values in most the complexes which

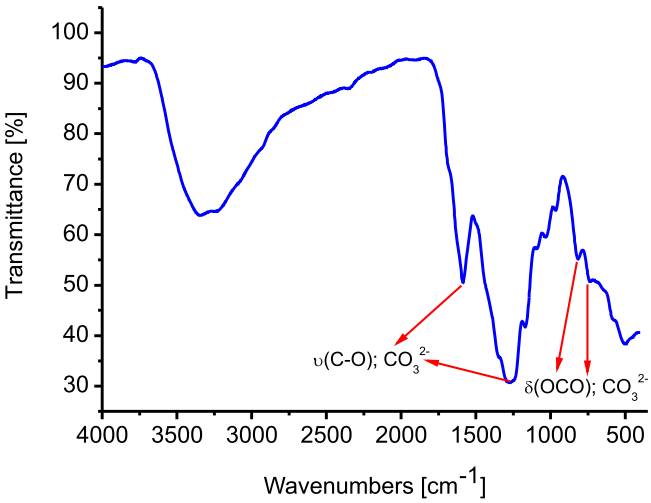

Figure 6. FT-IR spectrum of $[In(CH_3(CH_2)_4COO)_3]$ complex after calcinations at 350°C

Bereitgestellt von West-Pomeranian University of Technology Szczecin - Biblioteka Główna Zachodniopomorskiego | Heruntergeladen 16.01.20 10:41 UTC

Table 1. Kinetic thermodynamic parameters based on Horowitz-Metzger (HM) and Coats-Redfern (CR) methods

HM method*					CR method*				
E	Z	ΔS	ΔH	ΔG	E	Z	ΔS	ΔH	ΔG
70	1.91E+02	-209	63.6	225	52.8	9.44E+00	-234	46.4	227

*ΔG/kJmol^{-1}, ΔH/kJmol^{-1}, ΔS/Jmol^{-1}K^{-1}, Z/s^{-1}, E/kJmol^{-1}

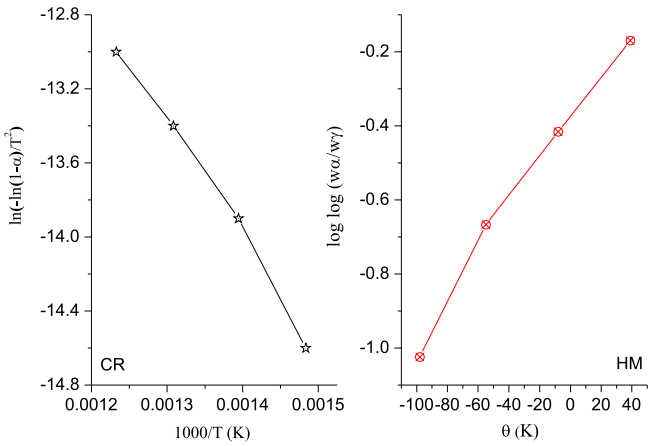

Figure 7. Kinetic thermodynamic CR and HM diagrams of $[In(CH_3(CH_2)_4COO)_3]$ complex

indicate that the decomposition reactions proceed with a lower rate than the normal ones. It is clear that the thermal decomposition process of studied complex is non-spontaneous, i.e., this complex is thermally stable.

XRD spectrum of the $[In(CH_3(CH_2)_4COO)_3]$ complex (Fig. 8) was measured within the 2θ = 4–80° range. This spectrum displayed that the synthesized indium(III) caproate precursor complex has a crystalline behavior. The new diffraction patterns presence in the spectrum of $In^{(III)}$ caproate complex are due to the formation of chelation between caproic acid and indium ions. The maximum diffraction patterns of $In^{(III)}$ complex is exhibited at 2θ = 16.8°. The particle size was calculated from XRD diagram by applying FWHM of the characteristic peaks using Deby-Scherrer equation[40], D = Kλ/βCosθ (where "D" term is the particle size of the crystal gain, "K" term is a constant (0.94 for copper grid), "λ" term is the X-ray wavelength (1.5406 Å), "θ" term is the Bragg diffraction angle and "β" term is the integral peak width. The particle size of the synthesized complex was calculated based on the highest 2θ in comparable with

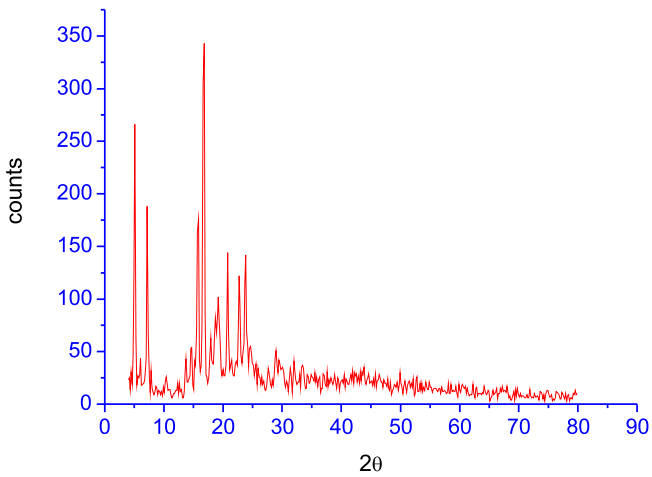

Figure 8. X-ray powder diffraction spectrum of $[In(CH3_(CH_2)_4COO)_3]$ comple

the other peaks. This value referred that the particle size exhibited at (70 nm) within nano scale range.

The examination of surface morphology of the $[In(CH_3(CH_2)_4COO)_3]$ complex was performed using SEM technique (Fig. 9). It can be seen that it gave a shape of the plates which are not compacted. This micrograph of indium(III) caproate complex indicated that the presence of well defined crystals free from any shadow of the impurities on the external surface. It is clearly from the SEM image that the synthesized $In^{(III)}$ complex, crystals were found to grow up from just a single molecule to several molecules in an aggregate distribution with particle sizes starting from a few nanometers to several hundred.

Figure 9. SEM image of $[In(CH_3(CH_2)_4COO)_3]$ complex

Characterization of In_2O_3 oxide NPs

This study describes the synthesis of In_2O_3 by the thermal decomposition route for the $[In(CH_3(CH_2)_4COO)_3]$ complex in static air. The discussions of the intermediate and the final thermal decomposition products were carried out by thermogravimetry, FT-IR spectroscopy, XRD, SEM, EDX, and TEM analyses. The analyses of these data show that the indium(III) caproate complex decomposed to In_2O_3 with the formation of an intermediate carbonate, $In_2(CO_3)_3$ compound. The In_2O_3 NPs with crystallite size in the nanosize range was formed after calcination at temperature 800°C. The suggested reaction occurring during the thermal decomposition of the indium(III) caproate complex is summarized below, according to TG/DTG and FT-IR results:

$$[In(CH_3(CH_2)_4COO)_3] \xrightarrow[\text{Static } O_2 \text{ gas}]{800\ ^oC} In_2O_3$$

FT-IR spectrum of the synthesized In_2O_3 NPs by the thermal decomposition technique is shown in Figure 10. There are three distinguish vibration bands at 589 and 665 cm^{-1} were existed, these are attributed to the ν(In–O)

Bereitgestellt von West-Pomeranian University of Technology Szczecin - Biblioteka Główna Zachodniopomorskiego | Heruntergeladen 16.01.20 10:41 UTC

stretching and δ(In–O–In) bending vibrations, respectively in cubic In_2O_3 structure[41–43]. This result support that the phase formation is complete for the as-prepared In_2O_3 NPs and there is no evidence for the presence of any organic impurities in the synthesized indium(III) oxide sample. On the other hand, the presence of broad band at 3434 cm^{-1} and medium band at 1642 cm^{-1} can be assigned to the stretching and bending vibrations of the ν(O-H) bands regarding water moisture.

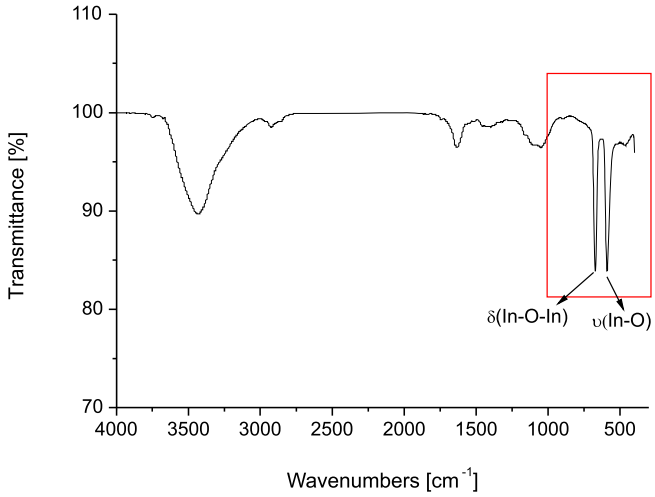

Figure 10. FT-IR spectrum of indium(III) caproate complex calcined at 800°C for 3 hrs

The electronic UV-Vis spectrum of synthesized In_2O_3 NPs was used to calculate the energy gap "E_g". The spectrum display absorption band at 347 nm (Fig. 11). The E_g value was estimated using the wood and Tauc plot[44] as referred in the following equation 3:

$$\alpha h\nu = A(h\nu - E_g)^{1/2} \quad \text{Eq.} \qquad (3)$$

where "A" term is a constant, "hν" term is the photon energy, and "E_g" term is the energy gap. Plotting $(\alpha h\nu)^2$ as a function of photon energy, and extrapolating the linear portion of the curve to the absorption equal to zero as shown in the insets of Figure 11 give the value of the direct band gap (*Eg*) to be 2.99 eV for the In_2O_3 sample calcined at 800°C. This value is less than that of ~3.6 eV for the In_2O_3 mentioned in the literature[45–47]. This value indicate the semiconductor behavior of In_2O_3 that can be used in photocatalyst applications[46, 47].

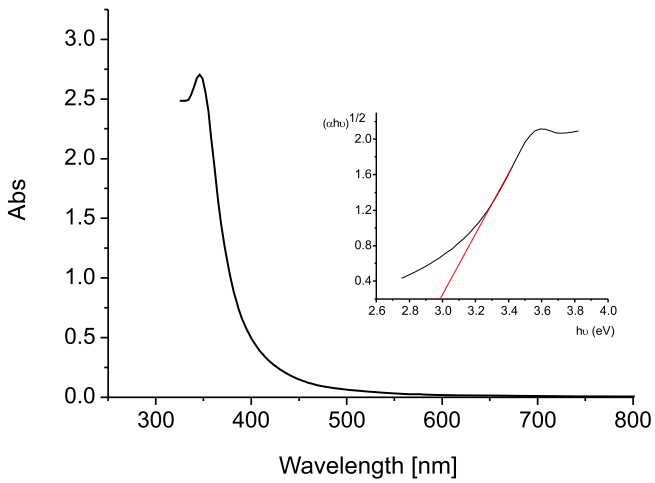

Figure 11. UV-Vis spectrum and energy band gap plots of the synthesized In_2O_3 NPs

The X-ray powder diffraction patterns of the indium(III) caproate complex after calcination at 800°C for 3 hrs is shown in Figure 12. The distinguish patterns attributed to cubic structure indexed on ICDD card 6–416[48]. Figure 12 shows the strong and sharp diffraction patterns reveal that the In_2O_3 NPs has a well crystalline structure. The diffraction patterns agree with those given in JCPD card 6–416 of cubic In_2O_3 reflections as 211, 221, 222, 400, 413, 440, and 622 planes. Calculation of particle size of indium oxide using Scherrer's equation gives 20 nm value, confirmed that the particle size of the In_2O_3 which was prepared by thermal decomposition method of indium(III) caproate complex is in the nanosize range < 100 nm.

The morphology of In_2O_3 NPs was investigated with SEM as shown in Figure 13. SEM micrograph (Fig. 13) reveals the overall appearance of indium(III) caproate complex calcined at 800°C for 3 hrs. The particles are nearly thick threads in shape has uniform size and distribution with symmetrical sizes, might be due to distribution of temperature during calcinations. It can be observed that product aggregation is constituted by many regular particles with a variety of porosity due to the evolution large amount of gases during synthesis. The porosity of In_2O_3 NPs facilitates and enhances the adsorption properties. The EDX analysis (Fig. 13) exhibited clear distinguish peaks of both indium and oxygen elements from the desired detected site. The atomic percentages of these elements are 82.71% and 17.29% for indium and oxygen, respectively.

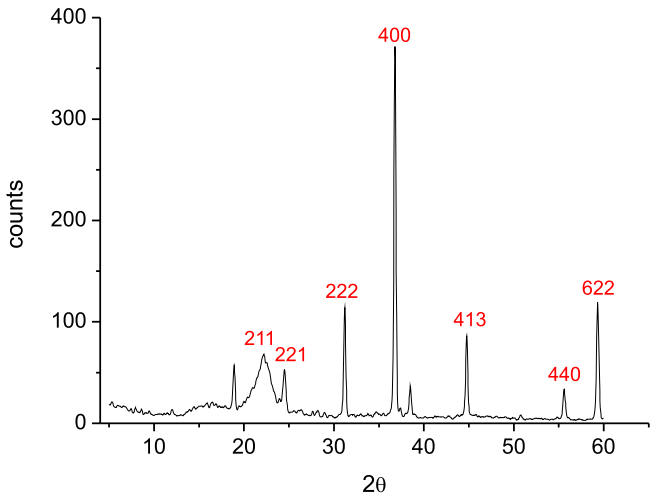

Figure 12. XRD diagram of the synthesized In_2O_3 NPs by calcined indium(III) caproate complex at 800°C for 3 hrs

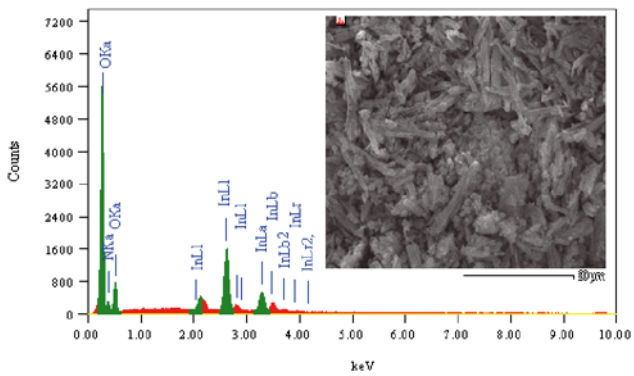

Figure 13. EDX spectrum and SEM image of the synthesized In_2O_3 NPs

Bereitgestellt von West-Pomeranian University of Technology Szczecin - Biblioteka Główna Zachodniopomorskiego | Heruntergeladen 16.01.20 10:41 UTC

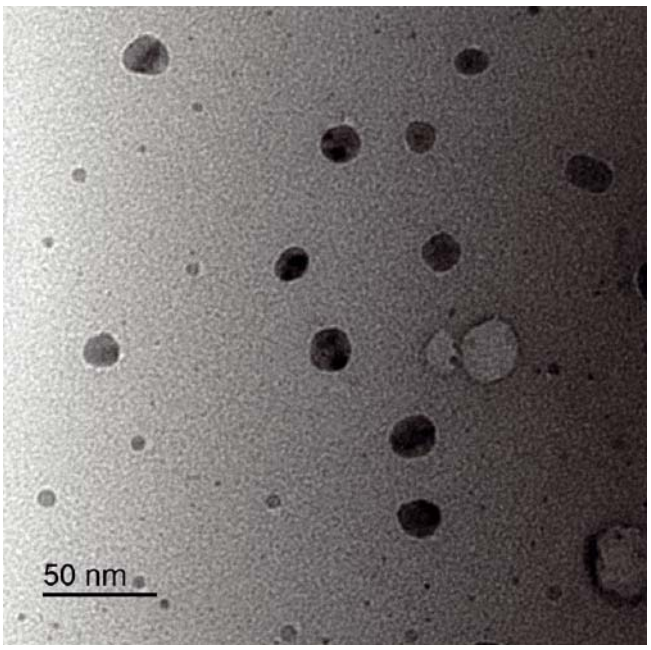

Figure 14. TEM image of the synthesized In_2O_3 NPs

Figure 14 shows a presented TEM image of the indium(III) caproate complex after calcination at 800°C for 3 hrs. The morphology of particles observed in the bright-field image is characterized by agglomerated NPs, most of them having a spheroidal shape. The particle size of the In_2O_3 NPs estimated by XRD was in agreement with the particle size obtained by TEM analysis (10–20 nm).

Photocatalytic degradation properties

In our study, the prepared In_2O_3 nanoscale size can be used as a photocatalyst smart material for the photodegradation of Congo Red (CR) and Crystal Violet (CV) organic dyes which are found in the wastewater of factories and rehabilitated for use in agriculture. The photocatalytic data of the In_2O_3 NPs confirm that the degradation of these dyes after 90 min for the UV-irradiation reached the maximum results ≈ 93%, and 95% for the CR and CV, respectively. The photocatalytic degradation experiments were operated at i-different contact time, ii-dose of In_2O_3 NPs adsorbent, and iii-effect of pH.

Effect of time

The effect of time on the degradation of CR and CV dyes onto In_2O_3 NPs adsorbent was investigated spectrophotometrically. These results are clearly displayed in Figure 15, which the degradable of industrial dyes (CR & CV) increased with the increasing of contact time of 90 min. The rate of adsorption is very fast at first with most of the compound being condensed during the first 45 minutes. It was found that more than >40% adsorption dyes (CR & CV) occurred at the 90 minutes. After that the rate of adsorption was found slow. This shows that it can be assumed that the balance is achieved after 45 minutes. This is mainly due to the saturation of the active site which does not allow more adsorption to occur. In general, the adsorption capacity and the color removal efficiency of the adsorbents are directly related to the contact time, thus increasing the adsorption of the surface while increasing the contact time due to increased contact with the dye molecules (CR & CV) with the adsorbed surface. However, it reaches a fixed value at a specific time. At this moment, the amount of dyes absorbed in a dynamic balance with a quantity not absorbed by the dyes, and after this time, the amount of adsorption of the dyes by the adsorbents is almost constant[49]. After adjust time the adsorbent was filtered from the solution for 15 min. The residual concentration of dye in solution was spectrophotometrically scanned at λ_{max} = 498 nm for CR and λ_{max} = 590 nm for CV (λmax) using a UV–Vis spectrophotometer. The % Adsorption was calculated according to Eq. (1).

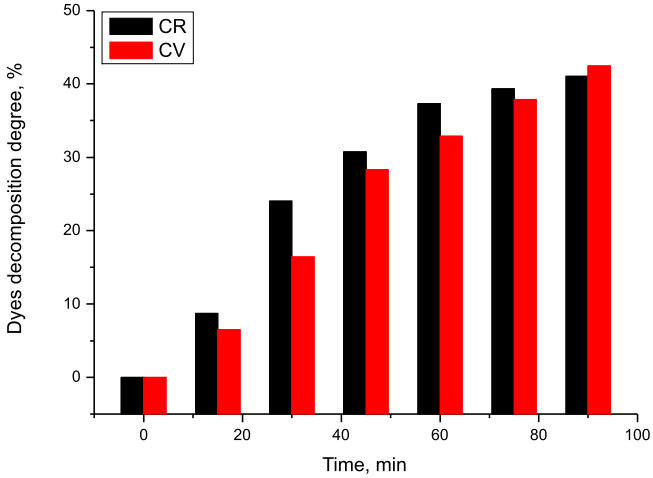

Figure 15. Dyes decomposition degree versus time of Congo Red (CR) and Crystal Violet (CV) dyes treated with In_2O_3 NPs at different contact time

Effect of In_2O_3 adsorbent doses

Degradation of the dyes (CR & CV) is strongly affected by the amount of In_2O_3 NPs adsorbents. The Congo Red (CR) and Crystal Violet (CV) adsorptions were studied on In_2O_3 NPs with a change in the adsorbents from 10 mg to 50 mg · L^{-1} at a 90 minutes continuous stirring rate with an optimal dye concentration of 50 mg · L^{-1}. It was observed from Figure 16 that by increasing the dose, the adsorption of dyes (CR & CV) increased the excellent amount of adsorbents. The maximum >60% and >70% for CR and CV dyes, respectively, are adsorbed at a dose of 50 mg of adsorbents. An additional increase in the absorbed dose reduces the absorption rate. This

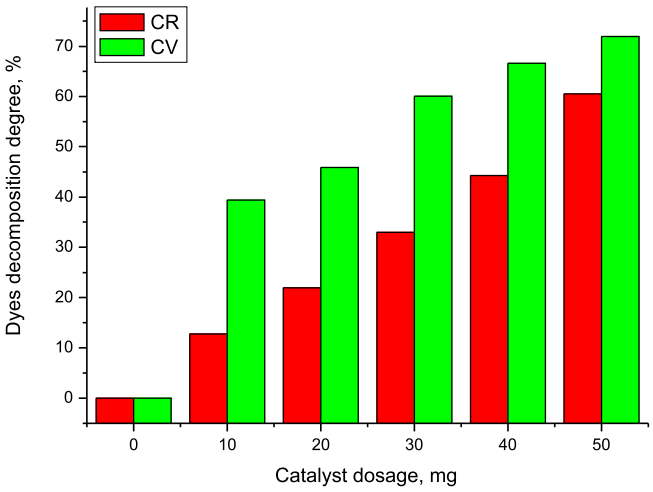

Figure 16. Dyes decomposition degree versus catalyst dosage of Congo Red (CR) and Crystal Violet (CV) dyes treated with different mass doses of In_2O_3 NPs

Bereitgestellt von West-Pomeranian University of Technology Szczecin - Biblioteka Główna Zachodniopomorskiego | Heruntergeladen 16.01.20 10:41 UTC

may be due to overfilling or aggregation of adsorption sites, resulting in a reduction in the available surface area of respected dyes[50].

Effect of pH value

The pH of the photocatalytic degradation process has a significant effect on the adsorption efficiency of most organic dyes. The effect of pH on adsorption of CR & CV dyes on In_2O_3 NPs was performed at 50 mg · L^{-1} of primary dye concentration with a 50 mg mass of In_2O_3 NPs adsorbent at 90 min of stirring rate at room temperature. As shown in Figure 17, In_2O_3 nanoparticles show maximum absorption of >79% of represented dyes at pH 12 which decreased at low acidic pH. This assures that low pH < 7 is unsuitable for dye absorption by In_2O_3 NPs.

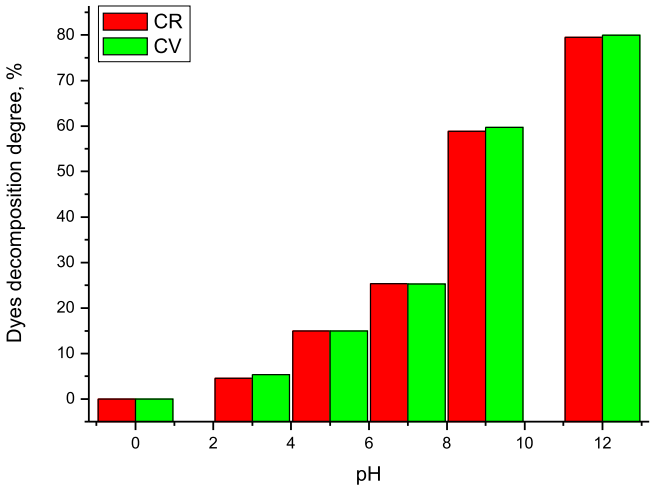

Figure 17. Dyes decomposition degree versus pH of Congo Red and Crystal Violet dyes treated with different In_2O_3 NPs at different pH

Based on the semi-conductor photovoltaic behavior of the catalyst, the radiation of this catalyst has a wide--band gap energy that leads to the electron pairing of the electron holes. These pairs then spread to the surface, where the electrons adsorbed hydroxide, the hole, and oxygen molecules, to form a hydroxyl radical. Before holes and electrons form on the surface, there is a great chance of recombination[51].

CONCLUSION

A nanoparticles of In_2O_3 resulting from the thermal decomposition of a $[In(CH_3(CH_2)_4COO)_3]$ complex as a precursor. The assignments of thermal analysis and FT-IR support that during the decomposition of the precursor complex a carbonate molecule is formed. The calcination of this precursor material at temperature 800°C gives rise to nanocrystalline particles of cubic In_2O_3 with sizes 10–20 nm. Energy band gap was calculated using UV-Vis spectroscopy. Photodegradation studies of CR and CV dyes on the surface of the In_2O_3 NPs were performed with various parameters such as contact time, effect of adsorbent dosage, and effect of pH. The results suggest that the In_2O_3 NPs are good photocatalyst for the removal of CR and CV dyes.

ACKNOWLEDGEMENTS

This work was funded by the Deanship of Scientific Research at "Imam Abdulrahman Bin Faisal University", through the Research Groups Program No. 2017-246-CED.

LITERATURE CITED

1. Cisneros, R.L., Espinoza, A.G. & Litter, M.I. (2002). Photodegradation of an azo dye of the textile industry. *Chemosphere*, 48(4), 393–399. https://doi.org/10.1016/S0045-6535(02)00117-0.
2. Lee, Y.H. & Pavlostathis, S.G. (2004). Decolorization and toxicity of reactive anthraquinone textile dyes under methanogenic conditions. *Water Res.*, 38(7), 1838–1852. https://doi.org/10.1016/j.watres.2003.12.028.
3. Xie, S., Ren, W., Qiao, C., Tong, K., Sun, J., Zhang, M., Liu, X. & Zhang, Z. (2018). An electrochemical adsorption method for the reuse of waste water-based drilling fluids. *Natural Gas Industry B*, 5(5), 508–512. https://doi.org/10.1016/j.ngib.2018.03.005.
4. Zhao, Z., Geng, C., Yang, C., Cui, F. & Liang, Z. (2018). A novel flake-ball-like magnetic Fe_3O_4/γ-MnO_2 meso-porous nano-composite: Adsorption of fluorinion and effect of water chemistry. *Chemosphere*, 209, 173–181. https://doi.org/10.1016/j.chemosphere.2018.06.104.
5. Radhakrishnan, A., Rejani, P., Khan, J.S. & Beena, B. (2016). Effect of annealing on the spectral and optical characteristics of nano ZnO: Evaluation of adsorption of toxic metal ions from industrial waste water. *Ecotoxicology and Environmental Safety*, 133, 457–465. https://doi.org/10.1016/j.ecoenv.2016.08.001.
6. Basheer, Al Arsh. (2018). New generation nano-adsorbents for the removal of emerging contaminants in water. *J. Molec. Liquids*, 261, 583–593.
7. Mehrotra, R.C. & Bohra, R. (1983). Metal Carboxylates, Academic Press, London.
8. Brusau, E.V., Pedregosa, J.C., Narda, G.E., Ayala, E.P. & Oliveira, E.A. (2004). Vibrational and thermal study of hexaaquatris (malonato) dieuropium (III) dihydrate. *J. Arg. Chem. Soc.*, 92(1/3), 43–52.
9. Gushchina, T.N. & Kotenko, G.A. (1983). *Koord. Khim.*, 12(3), 325.
10. Brzyska, W. & Paszkowska, B. (1998). Studies on the Thermal Decomposition of Rare Earth Caproates. *J. Thermal Anal.*, 51, 561–566. https://doi.org/10.1007/BF03340193.
11. Doyle, A., Felcman, J., Gambardella, M., Verani, C.N. & Tristao, M.L.B. (2000). Anhydrous copper(II) hexanoate from cuprous and cupric oxides. The crystal and molecular structure of $Cu_2(O_2CC_5H_{11})_4$. *Polyhedron*, 19(26/27), 2621–2627. https://doi.org/10.1016/S0277-5387(00)00568-4.
12. Pietsch, R. (1971). Untersuchungen über die extraktion von thorium, blei und eisen (III) als verbindungen der capronsäure. *Anal. Chim. Acta*, 53(2), 287–294. https://doi.org/10.1016/S0003-2670(01)82087-0.
13. Kolomiets, L.L., Lysenko, O.V. & Pyatnitskii, I.V. (1988). Photoelectric counter of disperse particles. *Z. Anal. Khim.*, 43(10), 1773.
14. Pyatnitskii, I.V., Kolomeits, L.L., Lysenko, O.V. & Sobko, M.G. (1990). *Z. Anal. Khim.*, 45(1), 56.
15. Kopacz, S., Szantula, J. & Pardela, T.Z. (1989). *Prikladoni Khim*, 62(11), 2535.
16. Mazouchi, M., Sarkar, K., Purahmad, M., Farid, S. & Dutta, M. (2018). Photoconduction mechanism of ultra-long indium oxide nanowires. *Solid-State Electronics*, 148, 58–62. https://doi.org/10.1016/j.sse.2018.07.003.
17. Du, X. & Man, B. (2018). Effect of growth temperature on the structural and optoelectronic properties of epitaxial indium oxide films. *J. Crystal Growth*, 499, 18–23. https://doi.org/10.1016/j.jcrysgro.2018.07.033.

Bereitgestellt von West-Pomeranian University of Technology Szczecin - Biblioteka Główna Zachodniopomorskiego | Heruntergeladen 16.01.20 10:41 UTC

18. Fuchs, F. & Bechstedt, F. (2008). Indium-oxide polymorphs from first principles, Quasi particle electronic states. *Phys. Rev*., 77(4), 55107–55109. https://doi.org/10.1103/PhysRevB.77.155107.

19. Li, C., Zhang, D., Han, S., Liu, X., Tang, T. & Zhou, C. (2003). Diameter-Controlled Growth of Single-Crystalline In_2O_3Nanowires and Their Electronic Properties. *Adv Mater*., 15(2), 143–146. https://doi.org/10.1002/adma.200390029.

20. Falcony, C., Kirtley, J.R., Dimaria, D.J., Ma, T.P. & Chen, T.C. (1985). Electroluminescence emission from indium oxide and indium-tin-oxide. *J. Applied Phys*., 58, 3556–3558. https://doi.org/10.1063/1.335730.

21. Mane, R.S., Pathan, H.M., Lokhande, C.D. & Han, S.H. (2006). An effective use of nanocrystalline CdO thin films in dye-sensitized solar cells. *Solar Energy*, 80(2), 185–190. https://doi.org/10.1016/j.solener.2005.08.013.

22. Zhang, D., Liu, Z., Li, C., Tang, T., Liu, X., Han, S., Lei, B. & Zhou, C. (2004). Detection of NO_2 down to ppb Levels Using Individual and Multiple In_2O_3 Nanowire Devices. *Nano. Lett*., 4(10), 1919–1924. https://doi.org/10.1021/nl0489283.

23. Karazhanov, S.Z., Ravindran, P., Vajeeston, P., Ulyashin, A., Finstad, T.G. & Fjellvag, H. (2007). Phase stability, electronic structure, and optical properties of indium oxide polytypes. *Phys. Rev. B*, 76, 75129–75131. https://doi.org/10.1103/PhysRevB.76.075129.

24. Lin, S.E. & Wei, W.C.J. (2008). Synthesis and Investigation of Submicrometer Spherical Indium Oxide Particles. *J. Am. Ceram. Soc*., 91(4), 1121–1128. https://doi.org/10.1111/j.1551--2916.2008.02266.x.

25. Chu, D.Y.P., Zeng, D.J. & Xu, J. (2007). Tuning the phase and morphology of In2O3 nanocrystals via simple solution routes. *Nanotechnology*. 18(43), 5605–5609.

26. Rey, J.F.Q., Plivelic, T.S., Rocha, R.A., Tadokoro, S.K., Torriani, I. & Muccillo, E.N.S. (2005). Synthesis of In_2O_3nanoparticles by thermal decomposition of a citrate gel precursor. *J. Nanopart. Res*., 7(2), 203–208. https://doi.org/10.1007/s11051-004-7899-7.

27. Geary, W.J. (1971). The use of conductivity measurements in organic solvents for the characterisation of coordination compounds. *Coord. Chem. Rev*., 7(1), 81–122. https://doi.org/10.1016/S0010-8545(00)80009-0.

28. Deacon, G.B. & Phillips, R.J. (1980). Relationships between the carbon-oxygen stretching frequencies of carboxylato complexes and the type of carboxylate coordination. *Coord. Chem. Rev*., 33, 227–250. https://doi.org/10.1016/S0010-8545(00)80455-5.

29. Alcock, N.W., Culver, J. & Roe, S.M. (1992). The Effects of Cations and Anions on the Ionic of the development of organic substitution methods. *J. Chem. Soc. Dalton Trans*., 1447.

30. Nakamoto, K. (1997). *Infrared and Raman Spectra of Inorganic and Coordination Compounds*, Wiley, New York.

31. Dunn, D.D. & Hall, R.H. (1975). *Purines, pyrimidines, nucleosides, and nucleotides: Physical constants and spectral properties*, in G.D. Fasman (Ed.), *Handbook of Biochemistry and Molecular Biology*, 3rd ed., Nucleic Acids, Vol. 1, CRC Press, Cleveland, Ohio, pp. 65–215.

32. Holm, R.H. & Cotton, F.A. (1958). Spectral Investigations of Metal Complexes of β-Diketones. I. Nuclear Magnetic Resonance and Ultraviolet Spectra of Acetylacetonates. *J. Am. Chem. Soc*., 80, 5658. https://doi.org/10.1021/ja01554a020.

33. Cotton, F.A. & Wilkinson, C.W. (1972). *Advanced Inorganic Chemistry*, 3rd Ed, Interscience Publisher, New York.

34. Refat, M.S., El-Korashy, S.A., Kumar, D.N. & Ahmed, A.S. (2008). FTIR, magnetic, ^{1}H NMR spectral and thermal studies of some chelates of caproic acid: Inhibitory effect on different kinds of bacteria. *Spectrochimica Acta Part A*, 70(1), 217–233. https://doi.org/10.1016/j.saa.2007.07.036.

35. Coats, A.W. & Redfern, J.P. (1964). Kinetic Parameters from Thermogravimetric Data. *Nature*, 201, 68–69.

36. Horowitz, H.W. & Metzger, G. (1963). A New Analysis of Thermogravimetric Traces. *Anal. Chem.*, 35, 1464–1468. https://doi.org/10.1021/ac60203a013

37. Zsako, J. (1968). Kinetic analysis of thermogravimetric data. *J. Phy. Chem*., 72(7), 2406–2411. https://doi.org/10.1021/j100853a022.

38. Sharp, J.H. & Wentworth, S.A. (1969). Kinetic analysis of thermogravimetric data. *Analyt. Chem*., 41(14), 2060–2062. https://doi.org/10.1021/ac50159a046.

39. Wendlandt, W.W. (1974). *Thermal Methods of Analysis*, John Wiley & Sons, New York, NY, USA, 2nd edition.

40. Cullity, B.D. (1978). *Elements of X-Ray Diffraction*, Second Edition, Addison-Wesley Publishing Company, ch. 5.

41. Nyquist, R.A. & Kagel, R.O. (1971). *In: Infrared Spectra of Inorganic Compounds*. Academic Press, New York, Vol. 4.

42. Keller, R.J. (1982). *In: The Sigma Library of FTIR Spectra*, Sigma Chemical, St. Louis, Vol. 2.

43. Mondal, A. & Ram, S. (2004). Reconstructive phase formation of ZrO_2nanoparticles in a new orthorhombic crystal structure from an energized porous $ZrO(OH)_2{\cdot}xH_2O$ precursor. *Ceramics International*, 30, 239. https://doi.org/10.1016/S0272-8842(03)00095-6.

44. Mott, N.F. & Davis, E.A. (1979). *Electronic Processes in NonCrystalline Materials*, 2nd ed., Clarendon Press, Oxford.

45. Li, C., Zhang, D., Han, S., Liu, X., Tang, T., Lei, B., Liu, Z. & Zhou, C. (2003). Synthesis, Electronic Properties, and Applications of Indium Oxide Nanowires. *Ann. N.Y. Acad. Sci*., 1006, 104–121. DOI: 10.1196/annals.1292.007.

46. Sreenivas, K., Rao, T. & Mansingh, A. (1985). Preparation and characterization of rf sputtered indium tin oxide films. *J. Appl. Phys*., 57, 384–392. https://doi.org/10.1063/1.335481.

47. Shigesato, Y., Takaki, S. & Haranoh, T. (1992). Electrical and structural properties of low resistivity tin-doped indium oxide films. *J. Appl. Phys*., 71, 3356–3364. https://doi.org/10.1063/1.350931.

48. Rey, J.F.Q., Plivelic, T.S., Rocha, R.A., Tadokoro, S.K., Torriani, I. & Muccillo, E.N.S. (2005). Synthesis of In_2O_3nanoparticles by thermal decomposition of a citrate gel precursor. *J. Nanoparticle Res*., 7, 203–208. https://doi.org/10.1007/s11051-004-7899-7.

49. Ghanizadeh, G.H. & Asgari, G. (2009). Removal of Methylene Blue Dye from Synthetic Wastewater with Bone Char**.** *Iran. J. Health Environ*., 2, 104–113. http://ijhe.tums.ac.ir/article-1-159-en.html.

50. Farzin, N., deh Hossein, N., Shahram, N., Asif, M., Inderjeet, T., Shilpi, A. & Kumar, G.V. (2016). Removal of malachite green from aqueous solutions by cuprous iodide–cupric oxide nano-composite loaded on activated carbon as a new sorbent for solid phase extraction: Isotherm, kinetics and thermodynamic studies. *J. Mol. Liq*., 213, 360–368. https://doi.org/10.1016/j.molliq.2015.07.058.

51. Tang, C.W. (2013). Study of Photocatalytic Degradation of Methyl Orange on Different Morphologies of ZnO Catalysts. *Modern Research in Catalysis*, 2, 19–24. http://dx.doi.org/10.4236/mrc.2013.22003.

Bereitgestellt von West-Pomeranian University of Technology Szczecin - Biblioteka Główna Zachodniopomorskiego | Heruntergeladen 16.01.20 10:41 UTC